Stability of gold bead tissue markers

Joel M. Miller Smith-Kettlewell Eye Research Institute, San Francisco, CA, USA

Ethan A. Rossi Smith-Kettlewell Eye Research Institute, San Francisco, CA, USA

Martin Wiesmair Smith-Kettlewell Eye Research Institute, San Francisco, CA, USA

Danielle E. Alexander Smith-Kettlewell Eye Research Institute, San Francisco, CA, USA

Orazio Gallo Smith-Kettlewell Eye Research Institute, San Francisco, CA, USA

Significant soft tissue features in the orbit and elsewhere are not resolved by MRI or any other imaging method. We describe a new method that uses tiny (~0.1 mm diameter) gold beads as markers to visualize movements of such tissues with high spatial resolution (~100 μm) and moderate temporal resolution (~100 ms). We describe bead fabrication, implantation, imaging, and image processing to extract three-dimensional bead coordinates. We then present results of an experiment to determine the stability of gold bead tissue markers (GBTMs) over time in normally moving orbital tissues. Most beads (76%) implanted in sclera, muscle, tendon, and connective tissue were highly stable over the 6-month measurement period. Beads that were judged unstable drifted only a few 100 μm. Bead flows with gaze suggested that posterior Tenon's capsule moves with the globe, that the lateral rectus belly may sideslip, producing "bridle forces," and that the posterior medial rectus pulley sling moves freely anteriorly and posteriorly, but hardly vertically, as required by the "coordinated active pulley" hypothesis. The GBTM method seems applicable to study such short time course phenomena as extraocular muscle (EOM) and connective tissue movement as a function of gaze and such long time course phenomena as myopic eye growth.

Keywords: gold beads, tissue markers, GBTM, orbital imaging, orbital anatomy, extraocular biomechanics, extraocular connective tissue, EOM pulleys

Introduction

Images of the orbit impressively demonstrate the high spatial resolution of modern MRI. The orbit is not buried deep in the body; hence, signal strength can be maximized by placing receiving coils (*surface coils*) close to structures of interest. Orbital fat, which produces strong signals, fills much of the space between the globe, extraocular muscles (EOMs), and bones, providing a background against which the later structures stand in sharp contrast. Orbital contents can be stabilized for imaging by providing awake, cooperative subjects with fixation targets (Miller, 1989). Finally, this small volume contains many fine features of scientific, clinical, and even aesthetic interest. Nevertheless, many important structures in the orbit, and elsewhere, cannot be resolved with MRI at its current level of development, and some cannot, in principle, be resolved with any method that images intrinsic features.

Leo Koornneef (1974, 1977, 1992) initiated the detailed study of connective tissue mechanics when he observed that localized entrapment of a muscle in an orbital blowout fracture caused general disturbance of binocular alignment, proposed that all the EOMs were tied together in complex ways, and set about describing extraocular connective tissues in detail. He used anatomic sectioning and staining, summarized in beautiful artist's renderings, to show the complex structure of normal human extraocular connective tissue (e.g., Figure 1). Perhaps, Koornneef's most important contribution was to show that orbital connective tissue structures are highly stereotyped, suggesting that they have specific biomechanical functions and therefore warrant study.

MRI and CT must discriminate weak signals emitted by small volumes of tissue (*voxels*) to approach the resolution of histological studies. Repeated scans can be averaged to increase signal-to-noise ratios until sessions are so protracted that subject movement becomes the dominant noise source (2–3 min is the practical limit for human orbital studies requiring fixation). Cadaveric samples can be scanned indefinitely but cannot reveal features such as those related to voluntary movement only evident in alert, behaving subjects.

doi: 10.1167/6.5.6 Received September 9, 2005; published April 27, 2006 ISSN 1534-7362

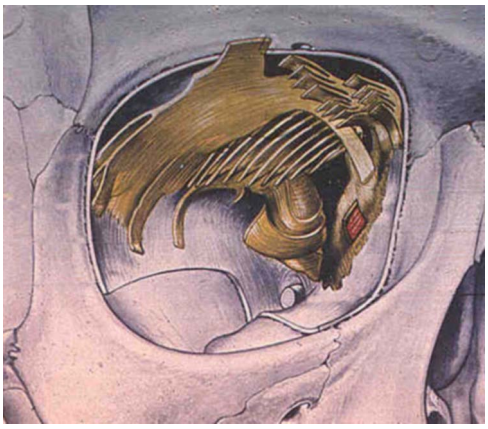

Figure 1. Connective tissue septa associated with the levator palpebre, the superior rectus, and the superior oblique muscles (modified from Koornneef, 1977).

In general, structures cannot be resolved unless they differ in contrast (e.g., muscle and sclera by MRI) or are separated by sufficient contrasting tissue (e.g., as orbital fat separates tendon and sclera in some gaze positions). These problems prevent, for example, visualization of EOM insertions where tendons are wrapped tightly around the histochemically similar sclera.

Finally, there are important data that no improvement in MRI or CT imaging resolution could provide. For example, the left panel of Figure 2 shows the now familiar pattern of EOM cross-section change as a function of gaze: As EOMs contract, their maximal cross sections increase and move posteriorly. This simple finding has formed the basis of objective diagnosis of EOM palsy (e.g., Demer, Miller, Koo, & Rosenbaum, 1994). A recent hypothesis about distinct functions for the histologically distinct *orbital* and *global* layers of EOM (Demer, Oh, & Poukens, 2000) suggests that there is significant shear across these layers; that is, although, in some circumstances, EOMs contract as shown in Figure 2B, in others, differential orbital–global contraction may occur, as schematized in Figure 2C. There are no macroscopically distinct tissues along the length of an EOM's belly, and thus there are no *intrinsic markers* that could be imaged to distinguish the two patterns of contraction. If *extrinsic markers* could be stably embedded in EOMs, the laminar shear hypothesis could be tested.

The first visualization in vivo of EOM paths was done in our laboratory, using portable medical X-ray equipment and trained monkeys with radiopaque markers implanted in their lateral rectus (LR) muscles (Miller & Robins, 1987; Miller, Robinson, Scott, & Robins, 1984). LR muscle paths were found to be stable with respect to the orbit for all gaze angles, a result that was surprising at the time but which has since been widely replicated in monkeys and humans using CT and MRI.

In the extension of this technique suggested by the right panel of Figure 2, we have implanted tiny gold beads in the orbit of a monkey trained to fixate and used a digital dental X-ray system to visualize the beads as functions of gaze and time. Gold is biocompatible and opaque to X-rays. Spheres as small as 0.1 mm are easily made and, with practice, can be handled and inserted into ocular tissues under surgical anesthesia.

It is possible to implant beads under visual guidance into anterior orbital tissues, and distinctive groups of beads can then be identified in reconstructed images. However, our main intent is to develop a method of visualizing deep tissues that cannot be directly visualized and so must be injected "blind," merely scattering enough markers in each

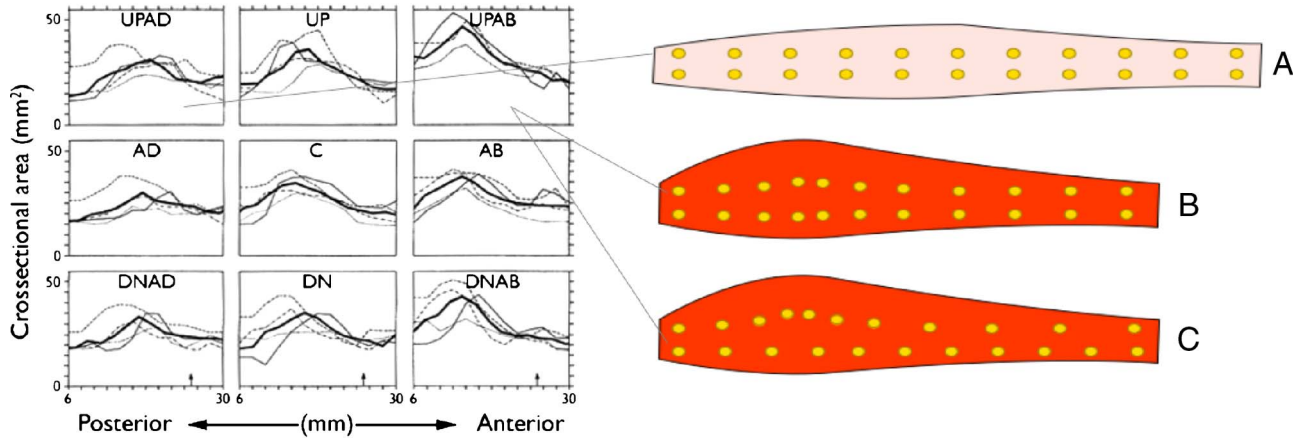

Figure 2. It is known that as an EOM contracts, its maximum cross section increases and the location of its maximum cross section moves posteriorly. The data on the left, adapted from Miller (1989), show LR cross sections by MRI for four normal humans (light lines) and their averages (dark lines), as a function of gaze (C = along orbital axis, AB = 37 deg abduction, AD = 37 deg adduction, UP = 37 deg elevation, DN = 37 deg depression, UPAB = 37 deg elevation and abduction, etc. Small arrows on abscissas give the location of the junction between globe and optic nerve). The panel on the right schematically shows (A) a relaxed muscle, (B) a contracted muscle in which upper and lower layers shorten similarly, and (C) a contracted muscle in which more of the cross-section change is due to contraction of upper layers. Gold spots in A, B, and C schematically suggest movements of specific bits of muscle tissue.

tissue of interest so that its movements can be visualized. Known tissues would be identified by the movements of the beads embedded in them and if bead density were high enough to "flesh out" its shape, by the configuration of the beads seen to be moving as a group.

We expect that *gold bead tissue markers* (GBTMs) will be uniquely useful for visualizing laminar shear (Demer et al., 2000), segmental stretching and contraction, and longitudinal movement in EOM and other muscles. GBTMs should also clarify movements of EOM pulleys and other extraocular connective tissues as a function of gaze. In a different application, GBTMs could map the pattern of regional growth in myopic, emmetropic, and hyperopic eyes of experimental animals.

If implanted gold beads tended to migrate, their utility as tissue markers would be limited to brief studies. There seems to be no consensus among surgeons on how such foreign bodies would behave in extraocular tissues. They might be expressed from some tissues, as a splinter is from skin; they might dislodge from soft, motile tissues to accumulate in quiescent regions; or they might stay where we put them. Here, we present the first results of this method in which we determine if GBTMs provide stable tissue referents or if they move about over time. Additionally, we present some preliminary findings on extraocular mechanics, which suggest the potential of the method.

Methods

Beads and bead injection

Gold wire was held in a pin vise and stroked with a small metal file, raining gold flakes onto a heat-resistant surface. An oxygen–propane microtorch was played over the flakes, melting them and allowing surface tension to form spheres with a narrow distribution of diameters. Beads were sorted with sieves and measured with calipers under a binocular microscope. We used beads of diameter 0.11–0.14 mm, which were the smallest we could handle from fabrication through implantation.

A simple injection device was designed so that hubless 29-gauge hypodermic needles (0.16–0.20 mm inside diameter) could be loaded with beads and introduced into tissues of interest (Figure 3). Beads were pushed out of the needle into the tissue with a tungsten stylet (0.15 mm diameter), cut to length so that when fully inserted, it reached the tip of the needle without extending beyond it.

All animal procedures followed a protocol approved by our USDA-authorized Animal Care and Use Committee. Aseptic surgery was conducted in an approved, dedicated surgical facility on site. A *Macaca mulatta* (rhesus monkey) was placed under surgical anesthesia by a veterinary anesthetist, who also monitored vital signs and provided life support throughout the procedure. Analgesics and antibiotics were provided according to an approved protocol. An operating microscope was used for all orbital work. In quadrants of interest, the conjunctiva was separated from the sclera at the limbus and blunt-dissected from the sclera back to the equator, allowing visualization of an expanse of sclera and anterior rectus muscles. The bead injector (Figure 3) was loaded with sterile gold beads, one or more of which were moved to the injector funnel and thence to the bore of the needle. The needle was then introduced into the tissue of interest, and the beads were injected. One, two, or three beads were injected at a time—different-sized bead groups facilitated identification across X-ray views and gazes and because several beads often entered the funnel together.

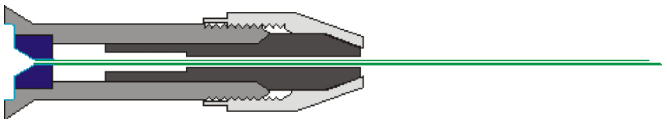

Figure 3. Bead injector. A 29-gauge hypodermic needle is held in a custom pin vise, which incorporates a funnel (at left) for loading beads into the needle, and a platform (the flat region just outside the funnel) on which beads can be stored for subsequent injections. A fitted tungsten stylet (not shown) is used to push beads into selected tissues. Needles are exchanged by loosening the collet.

We injected beads into anterior structures (EOM tendons and just beneath superficial sclera anterior to the equator) under direct visualization. Other bead injections targeted EOMs and connective tissues deeper in the orbit, which could not be visualized or verified at injection time, and would be identified later in the alert animal by the movements of embedded beads with eye rotation, as will become apparent.

Once several dozen injections had been completed, the conjunctiva was closed, antibiotic and anti-inflammatory ointment was applied to the eye, anesthesia was discontinued, and the animal was allowed to recover. The procedure was well tolerated, with the operated eye showing minimal swelling.

Bead visualization

After recovery, gold bead implants were visualized using a digital dental X-ray system (Gendex 765DC 65 kV, 7 mA, 0.4 mm source, Gendex Dental Systems, Des Plaines, IL; Sirona Sidexis digital sensor with 26 × 34 mm active area and 39 μm square pixels, Sirona Dental Systems LLC, Charlotte, NC) as the monkey performed an oculomotor fixation task for juice reward. For each gaze, we positioned the X-ray source at three different angles, with the digital X-ray sensor always perpendicular to the X-ray beam and close to the orbit (Figure 4).

Two views are sufficient to automatically reconstruct three-dimensional bead positions if matches across views are given, but a third view becomes necessary to distinguish false correspondences that might satisfy epipolar constraints

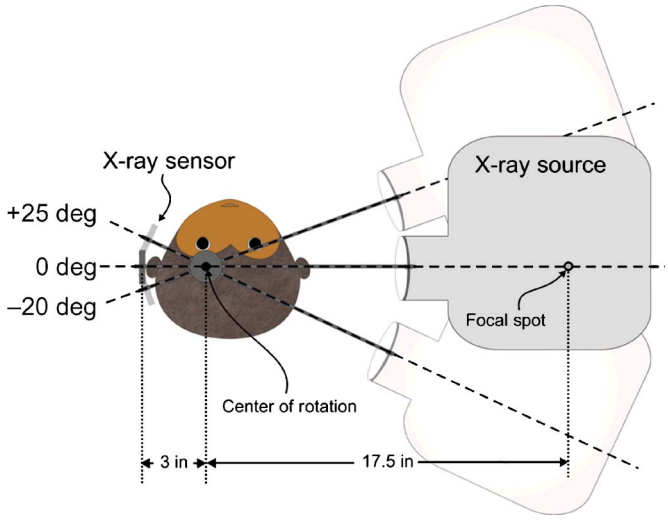

Figure 4. Arrangement of X-ray source and sensor, indicating views used in this study. The monkey faces an LED board (not shown), which elicits binocular fixations at 7.5 deg intervals over a 45 × 45 deg field. A cantilever holds the digital X-ray sensor perpendicular to the axis of the X-ray source and maintains sensor-to-source distance. Three views were imaged by rotating the cantilever around a vertical axis passing through the center of the orbit of interest (here, the left orbit).

(Hartley & Zisserman, 2003). The third view can also be employed to increase accuracy and resolve adventitious bead occlusions, which become more likely as the number of beads increases.

Here, we used three views, as shown in Figure 4. An X-ray exposure of 160-ms duration produced a clear bead image against shadows of the orbital bones (Figure 5; movement patterns will be analyzed below). Although imaging time is much shorter as compared with MRI, the GBTM method is still only useful for studying the orbital contents during periods of fixation, at least with our low-power X-ray equipment. Unintended motion during an exposure results in obvious doubled or smeared images, which can be discarded and recollected.

Image processing

A basic GBTM data set, sufficient to derive three-dimensional coordinates of an array of beads, consists of several *replications* of X-ray images taken from each of several *views*. The number of replications is chosen to reduce experimental error while maintaining reasonable data collection times. We did four replications.

For extraocular studies, it is of interest to study bead movement as a function of *gaze*. Data were collected in *primary gaze* (straight ahead) and in *secondary gaze positions* (i.e., at least one gaze coordinate = 0) at 7.5 deg gaze intervals over a 45 deg horizontal and vertical range (13 gazes). Finally, our principal aim being to study bead stability over time, we

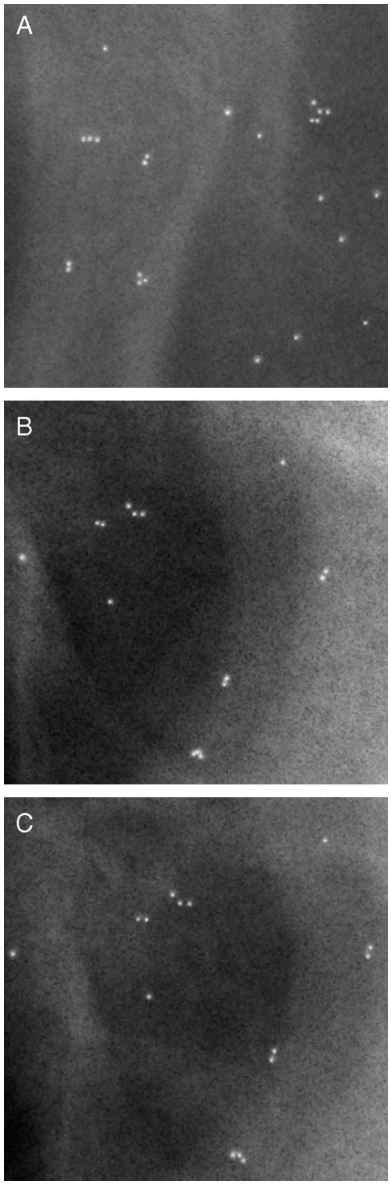

Figure 5. (A) Regions of two X-ray images from the early period and 0 deg (lateral) view, with the eye in two horizontal gazes separated by 7.5 deg. Anterior is to the left. Beads, implanted in and around the LR and MR, appear as white dots. Wispy lines are thickenings in the skull. Beads move generally horizontally with horizontal eye rotation, the direction and amount of movement determined by whether they are on the lateral or medial side of the eye, and on the tissue in which they are embedded. (B) Similar to Panel A, except viewed from +25 deg (anterolateral). A distinctive group of three beads and another group of two beads in the upper left quadrant of this figure can be readily identified with corresponding groups in the upper right quadrant of Panel A. Otherwise, correspondences are not obvious. (C) Similar to Panel B, except collected at the late period. Little drift in bead positions is apparent over the 6 months separating Panels B and C, and some of this is likely due to variability of gaze and view. Animated GIFs alternate between 2 gazes. Click on each panel to view the corresponding animation.

collected data sets at two times (*early* and *late*), separated by 6 months.

First, the two-dimensional coordinates of the bead images were extracted from the X-ray images: the background, common to all the views and gazes, was removed, Difference-of-Gaussian filters were convolved with each image to enhance the beads, and two-dimensional coordinates were extracted from maxima above a threshold. Then, beads were matched, first across views, based on knowledge of source and sensor locations, and then across gazes, with the aid of custom visualization software.

This calculation yielded eight sets of three-dimensional coordinates, four early and four late replications, for each gaze. View angles, sensor and source distances, and sensor orientations were not well controlled in these early studies (a new, more precise imaging apparatus is described in Figure 8). To remove errors caused by X-ray system alignment variation, we aligned the eight sets (as wholes) with affine transforms and a least squares criterion. Control of gaze, being voluntary, was only approximate, so that beads in a given structure (e.g., muscle) might be misaligned as a group with respect to the corresponding beads in another sample at the same nominal but somewhat different actual gaze. To remove these errors, we identified bead groups confined to a single structure and aligned them using only translation and a least squares criterion.

With three-dimensional coordinates as a function of gaze, testing hypotheses about relative tissue movement and stretching depends on being able to *segment* the bead flow into sets corresponding to different tissues of interest. Several segmentation methods can be used. One direct method relies on visualizing tissues of interest during surgery and placing distinctive bead configurations in known locations. Another would be to verify bead placements by postmortem sectioning or dissection, but we did not attempt this.

Where we cannot distinguish different tissues when we implant the beads, or postmortem, we use "intrinsic" methods of segmenting beads into different groups that correspond to different tissues. Our current intrinsic method is subjective. We plot sets of three-dimensional coordinates corresponding to adjacent gazes and view them as a movie. Perceptual grouping, based on *apparent motion* and *common fate* (Kaufman, 1974), seems to provide reasonable segmentations. Associated beads are then labeled (Figure 7B). Having the eye execute a wide range of movements, thereby maximizing relative bead motions, facilitates *common-fate segmentation*. It may be possible to develop an objective intrinsic method using *model-based segmentation*.

Results

The main aim of this study was to evaluate whether GBTMs reliably tag particular bits of extraocular tissue over time, but it will also be of interest to examine the patterns of bead movement with gaze to infer the identity of the tissues in which they are embedded so that we can say whether beads are more stable in some tissues than others. Finally, our data provide suggestive evidence for several biomechanically significant effects.

Fifty-four beads were identified across all three views and the seven vertical gazes at both early and late times. Three more were identified in all but one gaze at the late time and are shown in Figure 7 but were not statistically analyzed.

Bead stability over time

Following the alignment procedures described above, residual differences in bead positions across time would be due to actual bead drift plus uncorrected variations in gaze for a given attempted gaze. These estimates therefore somewhat overestimate bead drift alone.

Hotelling's T^2 test is the multivariate extension of Student's t test. Given two samples:

$$b_0 = (x, y, z)_{i,j,t_0},$$

the position of bead i, gaze j, at time t_0 and

$$b_6 = (x, y, z)_{i,j,t_6},$$

the position of bead i, gaze j, at time t_6, it tests the hypothesis

$$b_0 = b_6.$$

For each bead and gaze, we performed a T^2 test on the means of the replicates. It is possible for beads to have significant movement in from zero to seven tests. The distribution of the number of significant tests ($p < .01$, no multiple test correction) is shown in Figure 6. The 13 beads that showed significant drift in four or more gazes drifted between 0.08 and 0.26 mm (Figure 7A).

Bead flow with gaze

Figure 7B shows the orbit as the eye moved over a 45 deg horizontal range from (−22.5, 0 deg) through (+22.5, 0 deg)

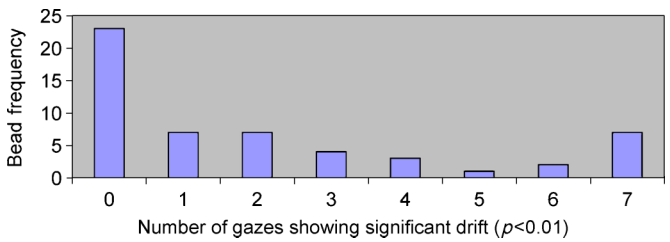

Figure 6. Number of beads showing significant drift in zero to seven gazes ($p < .01$). Only 13 beads showed significant drift in four or more gazes.

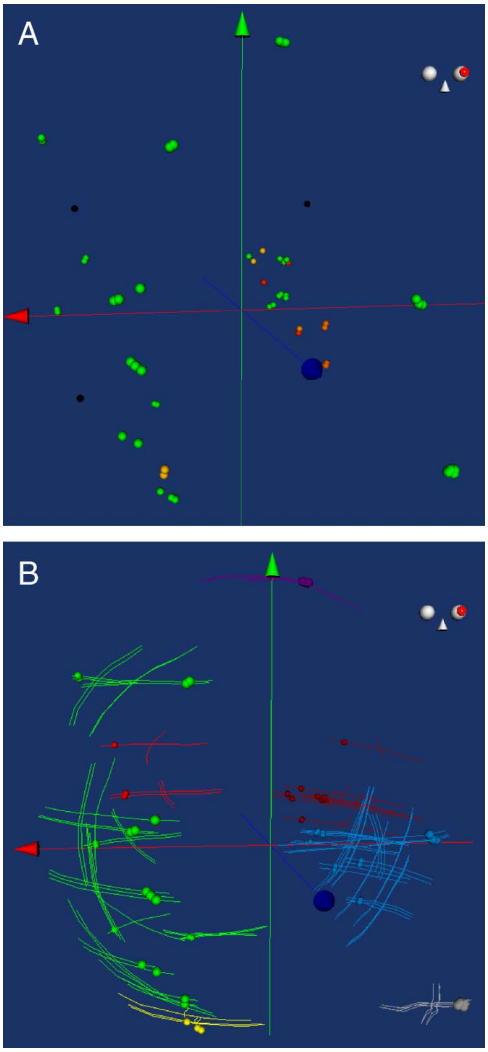

Figure 7. (A) Beads colored by stability over time. Green beads (n = 41) did not show significant drift in 4 or more gazes ($p < .01$). Significant drifts (n = 13) varied from 0.08 to 0.26 mm and are shown with colors grading from yellow through red. Black beads were not statistically analyzed. (B) Beads colored by known or inferred location. Green = globe; light blue = Tenon's capsule and the subcapsular space; light red = anterior MR; dark red = posterior MR pulley sling; yellow = IR; purple = SR–LP complex; grey = posterior LR. (Red axis arrows point anteriorly, green superiorly, and blue laterally. Beads are drawn twice-actual size. Icons in upper right corners show gaze of left, implanted eyes. VRML animations show eye rotating vertically from (0, −22.5 deg) to (0, +22.5 deg) in Panel A, and horizontally from (−22.5, 0) to (+22.5, 0) and vertically from (0, −22.5 deg) to (0, +22.5 deg) in Panel B. The objects in both panels are shown in perspective, not parallel, projection, and can be manipulated to different points of view. To see the animations and manipulate the objects, you must have VRML software installed on your computer. The free Cortona VRML Client [http://www.parallelgraphics.com/products/cortona/] works well. Click on the images to view the animations.)

and a 45 deg vertical range from (0, −22.5 deg) through (0, +22.5 deg). Beads are color coded according to the tissue in which we know or judge them to be embedded, the latter based on their movement as a function of gaze. A line through each bead traces its path over the range of eye movement. Some beads appear to wiggle, tracing jagged paths. We believe this to be an insignificant consequence of X-ray system misalignments, as described above.

It was relatively straightforward to segment beads to known structures by inspection:

- We implanted beads in the anterior globe under visual guidance. Thus, all beads moving on approximately circular paths in planes perpendicular to each axis of rotation that were also approximately equidistant from a common center, were segmented to the globe. (The reader can verify these assignments in Figure 7B by attending to horizontal rotations in superior or inferior view and vertical rotations in lateral or medial view.)
- No beads were implanted in sclera posterior to the globe equator. Thus, beads moving similarly to global beads but posterior to the globe equator must be in Tenon's capsule or the subcapsular space. It can be observed that these connective tissues rotate essentially with the globe.
- Several beads were injected under visual guidance in the anterior medial rectus (MR). These can be seen to move anteriorly with abduction and slightly superiorly with elevation, on paths in the anterior–medial orbit outside those of the global beads.
- Beads moving anteriorly with abduction and slightly inferiorly with elevation, on paths in the posterior–medial orbit outside those of the global beads, were assigned to extracapsular connective tissues associated with the posterior MR, in particular to the *posterior MR pulley sling* (see Demer, Miller, Poukens, Vinters, & Glasgow, 1995, Figure 10). This segmentation is inferred from the following features: (a) As can be seen in a superior or inferior view of Figure 7B, these beads cannot be in the posterior MR because they follow the arc of the globe, rather than heading posteriorly to the orbital apex. (b) As can be seen in a lateral or medial view of Figure 7B, during vertical eye rotation, they move vertically with the underlying capsular beads but only a fraction as much; hence they cannot be in the capsule. (c) They are farther from the center of rotation than global or capsular beads.
- Three beads inferior to the scleral beads moving anteriorly with elevation and slightly laterally with abduction were assigned to the inferior rectus (IR).
- A group of three beads in the superior orbit appear to lie at the lateral edge of the superior rectus–levator complex or in associated connective tissue (cf. Figure 1).
- A group of beads in the inferolateral posterior orbit move anteriorly with adduction and thus appear to be

in posterior LR. If so, the fact that they move superiorly with elevation suggests that the LR belly slides upward with elevation and downward with depression; that is, it slips around the globe to produce a "bridle effect."

A comparison of these tissue segmentations with the stability data suggests that the least stable beads (colored red and orange in Figure 7A) were in the capsule or the subcapsular space. In the latter case, their relative instability would not be surprising.

Conclusions

Beads and bead injection

Our method for fabricating beads is somewhat tedious but not unsuitable as a research method. Bead injection, however, needs to be improved. Transferring these dustlike bits of gold to the injector and from the injector platform into the needle is black art. Injection by stylet is clumsy in a surgical environment.

Bead visualization

Uncertainties of source and sensor positions allowed by our simple positioning system were removable by calculation, albeit with certain assumptions. For future work, we have constructed a more reliable positioning system (Figure 8). Stepping-motor control will make it practical to image the multiple views for a given gaze in rapid succession.

Figure 8. X-ray gantry designed to improve alignment and reproducibility of views. Platform (rectangular plate near top), turntable (large disk at top), and supports for X-ray source (lower right) and sensor (lower left) are positioned on two-dimensional linear bearings (near top) so that the center of rotation of the turntable passes through the eye (green sphere) or other object to be imaged. The X-ray source and the sensor are aligned with the eye. The turntable is rotated with a stepping motor under computer control.

Image processing

Developing an algorithm that identifies bead images across gazes, views, and replications has been proven to be challenging, mainly because all individual bead images look essentially the same. Matching across gazes can be facilitated by making the difference between adjacent gazes as small as necessary to disambiguate bead movements. Knowledge of X-ray source and sensor positions will be more useful in matching across views when those positions are better controlled (see Figure 8). Matching across replications would be facilitated by better control of eye position. In this connection, we are testing eye position monitors that do not require implants that would disturb extraocular tissues. There are also hints that should help with all matching, such as distinctive local groupings of beads, which would be invariant in three dimensions across views, replications, and (for tightly packed groups) gazes.

Bead stability over time

Gold beads are remarkably stable with respect to extraocular tissues in which they are placed. Of the beads that appeared to drift significantly in half or more of the gazes we analyzed, none drifted more than two bead diameters. Even this is probably an overestimate of drift because it includes any habitual fixation differences that developed over the 6 months of the experiment, which were not correctable by bead group translation (see above). Comparing Figure 7A with Figure 7B, we saw that the least stabile beads were located in the posterior capsule or subcapsular space.

To put this result in perspective, recall that there were good reasons to expect beads to be unstable. Tissue growth processes might have expelled them from sclera or muscle, for example, into surrounding connective tissues or fat. Frequent, fast saccadic eye movements might have shaken beads loose from motile tissues, causing them to accumulate in calmer places. None of these effects seem to be large over a 6-month period.

Tissue segmentation

In the current study of stability over time, the locations of anterior beads were known because they were injected under visual guidance during surgery. Other beads were segmented to tissues based on subjective assessment of positions and movements as a function of gaze. With further development of the GBTM method, we expect that bead localization in the latter cases will become more straightforward.

Subjective segmentation would certainly be improved by analyzing a wider range of gazes, which would provide additional opportunities for differential bead movements to become apparent. Automation of bead matching across replications, views, and gazes would make analysis of such large data sets more practical. Increasing the number of embedded beads would increase the probability that critical structures (e.g., orbital and global muscle layers in the posterior orbit) would be labeled and their relative movements visualized. It would also better "flesh out" tissue structures, making it possible to rely less on known anatomy and to describe previously unknown tissue relationships.

Subjective segmentation is not so bad when multiple observers agree and when data can be published as animations (e.g., Figure 7B) from which readers can make their own judgments. Nevertheless, automated segmentation would be more objective and less burdensome. We are considering various approaches to the *flow segmentation problem,* including model-based approaches that limit possible flows based on the types of tissues and motions (e.g., rigid rotating bodies and elongated musculoelastic "strands"; Pai et al., 2002) that might be present.

Extraocular mechanics

Although our focus in this work was development and validation of a new methodology, we have also obtained some preliminary results concerning extraocular mechanics.

We found that posterior Tenon's capsule rotates through angles essentially equal to those of sclera, showing that the globe is firmly attached to at least the posterior part of the capsule, as opposed to rotating within it. Given the substantial attachments of the capsule to the orbital wall (e.g., Koornneef, 1992), this implies that capsule elasticity is a substantial contributor to the globe's rotational stiffness.

Miller (1989) and Miller, Demer, and Rosenbaum (1993) demonstrated what should now be called *passive pulleys,* which stabilize posterior EOM paths relative to the orbit (e.g., for horizontal recti, they restrain vertical movement of the muscle bellies). Kono, Clark, and Demer (2002) have shown that, even as they stabilize rectus muscle paths against sideways movement, pulleys must, and do, move anteroposteriorly to enforce Listing's law in tertiary gaze. This is the concept of *coordinated active pulleys*. We have visualized tissues, identified as the posterior MR pulley sling, that displace freely during horizontal eye rotation but minimally during vertical eye rotation. Vertical stability of these tissues is impressive relative to the full vertical movement of adjacent capsular tissues.

If we correctly identified the posterior LR, then we have shown, unexpectedly, that this muscle sideslips upward with globe elevation and downward with depression. Such movements, a consequence of pulley elasticity, might allow the LR to develop a so-called "bridle force," further elevating the eye in elevation and depressing it in depression. It had been thought that the oculomotor system avoided such unstable mechanics (Miller, 1989).

Acknowledgments

This research was supported by National Institutes of Health Grant EY-13443 to J. M. Miller.

Thanks to Blair Christian, PhD, and Rudy Guerra, PhD, Department of Statistics, Rice University, for statistics consulting.

Commercial relationships: none.
Corresponding author: Joel M. Miller.
Email: jmm@eidactics.com.
Address: Smith-Kettlewell Eye Research Institute, 2318 Fillmore Street, San Francisco, CA 94115-1813, USA.

References

Demer, J. L., Miller, J. M., Koo, E. Y., & Rosenbaum, A. L. (1994). Quantitative magnetic resonance morphometry of extraocular muscles: A new diagnostic tool in paralytic strabismus. *Journal of Pediatric Ophthalmology and Strabismus, 31,* 177–188. [PubMed]

Demer, J. L., Miller, J. M., Poukens, V., Vinters, H. V., & Glasgow, B. J. (1995). Evidence for fibromuscular pulleys of the recti extraocular muscles. *Investigative Ophthalmology & Visual Science, 36,* 1125–1136. [PubMed]

Demer, J. L., Oh, S. Y., & Poukens, V. (2000). Evidence for active control of rectus extraocular muscle pulleys. *Investigative Ophthalmology & Visual Science, 41,* 1280–1290. [PubMed] [Article]

Hartley, R., & Zisserman, A. (2003). *Multiple view geometry in computer vision*. Cambridge: Cambridge University Press.

Kaufman, L. (1974). *Sight and mind*. New York: Oxford University Press.

Kono, R., Clark, R. A., & Demer, J. L. (2002). Active pulleys: Magnetic resonance imaging of rectus muscle paths in tertiary gazes. *Investigative Ophthalmology & Visual Science, 43,* 2179–2188. [PubMed] [Article]

Koornneef, L. (1974). The first results of a new anatomical method of approach to the human orbit following a clinical enquiry. *Acta Morphologica Neerlando-Scandinavica, 12*(4), 259–282. [PubMed]

Koornneef, L. (1977). *Spatial aspects of orbital musculofibrous tissue in man*. Amsterdam and Lisse: Swets & Zeitlinger.

Koornneef, L. (1992). Orbital connective tissue. In W. Tasman (Ed.), *Duane's foundations of clinical ophthalmology* (Vol. 1, pp. 1–23). Philadelphia: J. S. Lippincott Company.

Koornneef, L. (1991). Orbital connective tissue. In W. Tasman & E. A. Jaeger (Eds.), *Duane's foundations of clinical ophthalmology* (Rev. ed., Vol. 1). Philadelphia: J. B. Lippincott.

Miller, J. M. (1989). Functional anatomy of normal human rectus muscles. *Vision Research, 29,* 223–240. [PubMed]

Miller, J. M., Demer, J. L., & Rosenbaum, A. L. (1993). Effect of transposition surgery on rectus muscle paths by magnetic resonance imaging. *Ophthalmology, 100,* 475–487. [PubMed]

Miller, J. M., & Robins, D. (1987). Extraocular muscle sideslip and orbital geometry in monkeys. *Vision Research, 27,* 381–392. [PubMed]

Miller, J. M., Robinson, D. A., Scott, A. B., & Robins, D. (1984). Side-slip and the action of extraocular muscles. In *Association for Research in Vision and Ophthalmology* (p. 182). Sarasota, FL: Investigative Ophthalmology and Visual Science.

Pai, D. K. (2002). STRANDS: Interactive Simulation of Thin Solids using Cosserat Models. *Computer Graphics Forum, 21*(3).